Acta Cryst. (1998). B**54**, 912–920

Charge Density Study of 2-Pyridone

H. W. Yang and B. M. Craven*†

Department of Crystallography, University of Pittsburgh, Pittsburgh, PA 15260, USA. E-mail: craven@grove.iup.edu

(*Received 24 April 1997; accepted 6 May 1998*)

Abstract

The crystal structure of 2-pyridone has been redetermined from high-resolution X-ray data collected at 123 K. The molecule is in the lactam form. Bond lengths (corrected for rigid-body libration) and angles have been determined with s.u.'s of 0.001 Å and 0.1°, respectively. The hydrogen-bonded cyclic dimers which occur in the vapor and in solution are absent in the crystal where molecules are linked by N—H···O hydrogen bonds to form puckered chains. There also appears to be a weaker C—H···O interaction (H···O, 2.57 Å) and weak C—H···π or van der Waals interactions occurring on both sides of the pyridone ring. Following a refinement of the structure assuming Stewart's rigid pseudo-atom model, the electronic charge density distribution in the crystal and its Laplacian have been calculated for atoms at rest. The total electrostatic potential has been mapped for an isolated molecule and the molecular dipole moment has been determined [8.8 (19) D; 1D $\simeq$ 3.33564 $\times$ 10^{-30} C m]. Critical points in the electron density have been located for the bonds within the molecule and for the molecular interactions cited above. For the C—H···π interactions, only the spherical components of the valence density for the pyridone ring atoms contribute effectively at the critical points. Hence, these may be better described as van der Waals interactions.

1. Introduction

2-Pyridone (2-oxopyrimidine or α-pyridone, C_5H_5NO; Fig. 1) has long been of interest because it exhibits lactam–lactim tautomerism (Fig. 2). The lactam form occurs in the crystal structure of 2-pyridone (Penfold, 1953*a*) and in crystals of related molecules such as 2-thiopyridone (Penfold, 1953*b*; Ohms *et al.*, 1982), 5-chloro-2-pyridone (Kvick & Booles, 1972) and 4-hydroxy-2-pyridone (Low & Wilson, 1983), but the lactim form occurs in crystals of 6-chloro-2-hydroxypyridine (Kvick & Olovsson, 1968). It should be noted that in the 1:1 molecular complex of 2-pyridone and 6-chloro-2-hydroxypyridine (Almlöf *et al.*, 1971), each molecule has the tautomeric form that exists in its own crystal structure. Since lactam groups occur in *cis*-peptides and in the pyrimidine and purine bases of the nucleic acids, 2-pyridone has been studied as a model for biological processes involving tautomerism and proton transfer. Beak (1977) pointed out that for the isolated molecule in the vapor, the lactim form of 2-pyridone had a slightly lower free energy. In solution, the lactam form is favored. IR, UV and Raman spectroscopy indicate that in solution there is an equilibrium between monomers and dimers of the lactam form (Fujimoto *et al.*, 1981). Dimers are favored in nonpolar solvents such as benzene. From *ab initio* molecular orbital calculations, Field & Hillier (1987) concluded that the lactam form

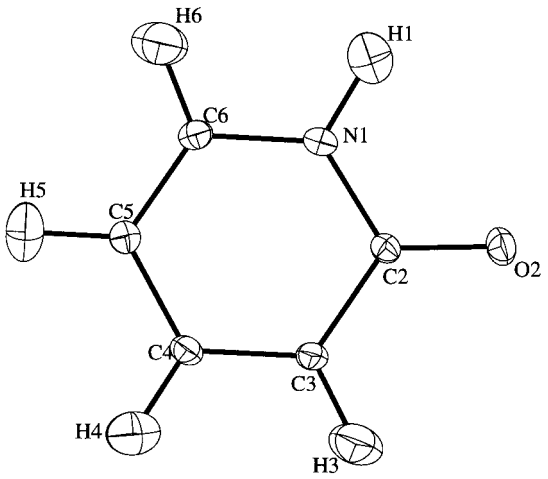

Fig. 1. Atomic nomenclature for 2-pyridone and the representation of atomic mean-square displacements as ellipsoids with 50% probability for enclosing each atom (Johnson, 1976).

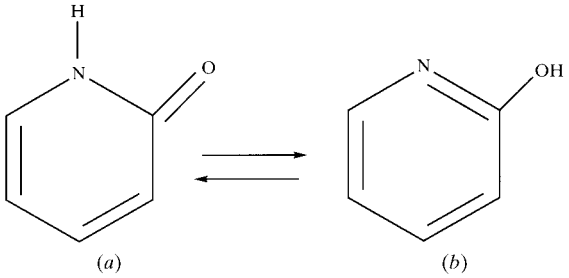

Fig. 2. Lactam/lactim tautomerism: (*a*) 2-pyridone and (*b*) 2-hydroxypyridine.

† New address: Department of Chemistry, Indiana University of Pennsylvania, Indiana, PA 15705, USA.

was favored in hydrogen-bonded cyclic dimers and in hydrogen-bonded complexes of 2-pyridone with water. Rotationally resolved fluorescence excitation spectra have been obtained for 2-pyridone in supersonic jets of the vapor (Held & Pratt, 1990; Held *et al.*, 1991; Held & Pratt, 1992). Rotational parameters indicate that monomeric 2-pyridone has the lactam form and is planar in the ground state, but in the excited state the molecule exists in two different puckered conformations. Cyclic dimers of the lactam tautomer were found to be hydrogen bonded with an N···O distance of 2.77 Å in the ground state and 2.87 Å in the excited S_2 state.

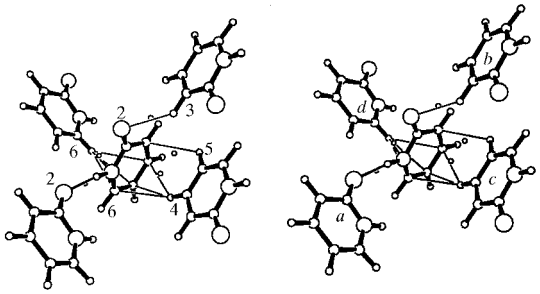

Fig. 3. Stereoview of the crystal environment of the central molecule (Johnson, 1976). The view is along the +*b* direction with **a** from left to right and **c** up the page. Circles of decreasing radii represent O, N, C and H atoms. The smallest circles represent critical points for the weak intermolecular interactions. Thin lines represent the shortest interatomic vectors for these interactions (Table 3*d*). In the left-eye view certain ring positions are numbered according to Fig. 1. In the right-eye view molecules are denoted by letters according to the symmetry operations in Table 3(*d*). The central molecule forms the asymmetric unit (Table 1).

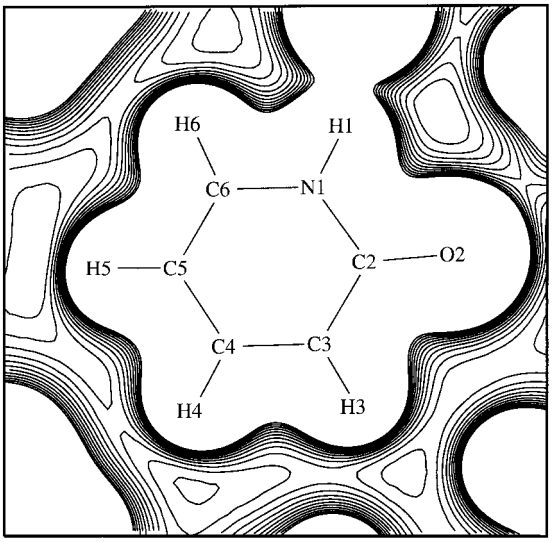

Fig. 4. The total electron density in the best molecular plane for atoms at rest. Contours are at intervals of 0.01 e Å^{-3} beginning at 0.01 e Å^{-3}. The sections are all parallel to the best molecular plane (Table 3*e*). There is connecting density to neighboring molecules, but these connections are not at true saddle points because the neighboring atoms are not close enough to this section.

The crystal structure of 2-pyridone was first determined at room temperature by Penfold (1953*a*), using eye-estimated intensities measured on *hk*0 and *h*0*l* Weissenberg films. The positions of all H atoms were obtained from difference Fourier maps. The crystal structure is orthorhombic with space group $P2_12_12_1$ and has one molecule in the asymmetric unit. The molecules pack in a herringbone pattern with N—H···O hydrogen bonds (N···O, 2.77 Å) linking molecules in puckered chains along the *c* direction (Fig. 3). Our X-ray diffraction data have been collected at reduced temperature (123 K) and high resolution (sin $\theta/\lambda < 1.08$ Å^{-1}) in order to obtain the molecular geometry more precisely and also to obtain details of the charge density distribution and related electrostatic properties.

2. Experimental

A sample of 2-pyridone was purchased from Sigma Chemical Co., St Louis.† For X-ray data collection, a crystal (0.50 × 0.30 × 0.30 mm) was selected directly from this sample. It was mounted on a glass fiber with the crystal *c* axis close to the φ axis of an Enraf–Nonius CAD-4 diffractometer. All 2630 reflections in an octant with sin $\theta/\lambda < 1.08$ Å^{-1} were collected using Nb-filtered Mo $K\alpha$ radiation. The crystal was maintained at 123 K by a stream of cold nitrogen gas with the temperature monitored by a thermocouple in the cold stream ~8 mm upstream from the crystal. To minimize ice formation on the crystal, the diffractometer was sealed in a box with a positive pressure of dried air.

The crystal lattice parameters [a = 13.585 (2), b = 5.806 (3), c = 5.603 (2) Å] were obtained by a least-squares fit of $\sin^2\theta$ values for 22 reflections occurring in the range $13.0 < \theta < 22.0°$. In order to correct for any crystal miscentering, each reflection was measured at four equivalent positions (two with $+\theta$ and two at $-\theta$). The X-ray intensities were measured by $\omega/2\theta$ scans with ω-scan width $(0.80 + 0.35 \tan\theta)°$ and scan speed ~3.3° min^{-1}, with maximum time 90 s per reflection. The detector aperture width was $(4.0 + 0.5\tan\theta)$ mm. The intensities of three standard reflections (105, 360 and 910) monitored after every 6000 s were found to have a maximum variation of 3%. Using computer programs by Blessing (1987), the integrated intensities were estimated from the scan profiles, each of which was recorded at 48 equal intervals. No absorption corrections were applied.

The structure was initially redetermined by direct methods (Sheldrick, 1985) and then refined by conventional full-matrix least-squares methods using the *POP* computer program (Craven *et al.*, 1996). The residual minimized in this and subsequent refinements was $\sum w\Delta^2$, where $w = \{\sigma^2(F_o^2) + 0.0004F_o^4\}^{-1}$ and $\Delta =$

† The catalogue has this compound entered incorrectly as the lactim 2-hydroxypyridine.

Table 1. *Atomic parameters*

(*a*) Positional and displacement parameters for C, N and O atoms. These are the values from the final refinement which included the electron population parameters. Fractional coordinates are $\times 10^4$ and mean-square displacements, defined by the expression $T = \exp(-2\pi^2 \Sigma_i \Sigma_j h_i h_j a^{*i} a^{*j} U^{ij})$, are in units of $Å^2 \times 10^4$.

Atom	x	y	z	U^{11}	U^{22}	U^{33}	U^{12}	U^{13}	U^{23}
N1	−1912 (1)	2146 (1)	−1778 (1)	116 (2)	122 (2)	139 (2)	−18 (2)	−8 (2)	−19 (2)
C2	−1376 (1)	2096 (1)	311 (1)	104 (2)	120 (2)	128 (2)	−17 (2)	5 (2)	9 (2)
O2	−1508 (1)	516 (2)	1793 (2)	155 (3)	166 (3)	191 (3)	−32 (2)	5 (3)	63 (3)
C3	−689 (1)	3958 (1)	598 (1)	119 (2)	148 (2)	119 (2)	−33 (2)	8 (2)	0 (2)
C4	−615 (1)	5668 (1)	−1077 (1)	135 (2)	136 (2)	139 (2)	−39 (2)	4 (2)	−4 (2)
C5	−1207 (1)	5643 (1)	−3156 (1)	146 (2)	144 (2)	136 (2)	−17 (2)	−1 (2)	18 (2)
C6	−1841 (1)	3839 (1)	−3452 (1)	125 (2)	154 (2)	122 (2)	−4 (2)	−16 (2)	−6 (2)

(*b*) Positional and displacement parameters for the H atoms. These values were obtained from an initial conventional refinement and subsequently adjusted, making use of neutron diffraction results for benzamide (Gao *et al.*, 1991). Positional parameters are fractional coordinates $\times 10^3$ and mean-square displacements are in units of $Å^2 \times 10^3$. The U_{iso} values were obtained from the conventional refinement.

Atom	x	y	z	U^{11}	U^{22}	U^{33}	U^{12}	U^{13}	U^{23}	U_{eq}	U_{iso}
H1	−241	83	−208	25	24	37	−9	−2	−5	29	29
H3	−22	404	217	28	43	22	−4	−8	−1	31	28
H4	−8	704	−82	30	28	39	−14	0	−3	32	30
H5	−116	698	−451	39	30	30	0	2	13	33	35
H6	−234	361	−494	29	43	25	−1	−10	−3	32	40

(*c*) Electron population parameters. Higher multipole population parameters are $\times 10$. These terms and their corresponding normalizing factors are as listed by Epstein *et al.* (1982). Terms for all atoms are referred to the Cartesian crystal axes. The final κ values obtained were 1.009 (6), 0.998 (8) and 0.964 (5) for C, N and O, respectively.

Atom	p_v	d_1	d_2	d_3	q_1	q_2	q_3	q_4	q_5
N1	5.04 (9)	−3 (2)	−1 (2)	4 (2)	−3 (2)	2 (2)	1 (2)	3 (3)	0 (2)
C2	3.96 (9)	3 (2)	9 (3)	3 (3)	−5 (2)	20 (2)	8 (3)	−14 (3)	−3 (2)
O2	6.48 (8)	5 (2)	−14 (2)	3 (3)	5 (2)	6 (2)	4 (3)	−3 (3)	2 (2)
C3	4.26 (8)	−3 (2)	2 (3)	1 (3)	−3 (2)	11 (3)	7 (3)	−12 (3)	6 (2)
C4	3.99 (7)	−4 (3)	0 (3)	5 (3)	−9 (2)	14 (3)	10 (3)	−10 (3)	7 (2)
C5	4.00 (7)	0 (3)	3 (3)	6 (3)	−12 (2)	11 (3)	12 (3)	−4 (3)	3 (2)
C6	3.99 (7)	1 (3)	−4 (3)	2 (3)	−2 (2)	14 (3)	10 (3)	−9 (3)	5 (2)
H1	0.76 (3)	11 (3)	11 (3)	2 (3)					
H3	0.83 (3)	−7 (3)	−5 (4)	−14 (3)					
H4	0.88 (3)	−12 (3)	−12 (3)	−3 (3)					
H5	0.93 (3)	0 (3)	−14 (3)	19 (3)					
H6	0.88 (3)	13 (3)	2 (3)	11 (3)					

Atom	o_1	o_2	o_3	o_4	o_5	o_6	o_7
N1	7 (2)	−7 (2)	5 (2)	−3 (6)	14 (2)	13 (2)	2 (2)
C2	−1 (2)	7 (2)	−20 (3)	5 (7)	−15 (2)	−13 (3)	−13 (3)
O2	1 (2)	2 (2)	1 (2)	3 (6)	2 (2)	2 (2)	6 (2)
C3	1 (2)	−11 (2)	11 (3)	3 (6)	19 (2)	10 (3)	4 (3)
C4	−11 (2)	8 (2)	−11 (3)	10 (7)	−17 (2)	−15 (3)	−10 (3)
C5	10 (2)	−3 (3)	10 (3)	1 (7)	13 (2)	15 (3)	9 (3)
C6	−9 (2)	1 (2)	−19 (3)	10 (7)	−18 (2)	−25 (3)	−8 (3)

$||F_o|^2 - |F_c|^2|$ and all 2630 reflections were included. This refinement gave $R(F^2) = 0.066$, $wR(F^2) = 0.096$ and g.o.f. = 1.66.† Before proceding with the charge density analysis, the H-atom parameters were modified to give the values listed in Table 1(*b*). The H-atom positions were adjusted to give C—H and N—H bond lengths corresponding to those obtained by neutron diffraction for the chemically related molecule of benzamide (Gao *et al.*, 1991). The values were 1.086 Å for the C—H bond lengths and 1.040 Å for N—H. Mean-square anisotropic displacement parameters for the H atoms were estimated as the sum of external and internal mean-square displacements. The external values were obtained by first fitting the heavier-atom U^{ij} to a rigid-body model (Schomaker & Trueblood, 1968). A good least-squares fit was obtained with $wR(U) = 0.027$ and g.o.f. 1.06. The resulting molecular T, L and S tensor components (Table 2) were then used to calculate the external U^{ij} for the H atoms. The internal U^{ij} for the H atoms were obtained by assuming the transferability of values reported for benzamide at 15 K from analysis of neutron

† $R(F^2) = \sum \Delta / \sum F_o^2$; $wR(F^2) = \{\sum w\Delta^2 / \sum wF_o^4\}^{1/2}$; g.o.f. = $\{\sum w\Delta^2/(N_{obs} - N_{var})\}^{1/2}$.

Table 2. *Molecular framework rigid-body vibrations*

Molecular translational, librational and cross-tensor components have been obtained by fitting U^{ij} for the C, N and O atoms, assuming a rigid-body model. The molecular tensor components are given with respect to the axes of the principal moments of inertia of the molecular framework and with the origin at its center of mass. The principal moments of inertia are 269.2, 180.2 and 89.0 Da. The largest moment of inertia is along the Cartesian z axis which is the normal to the ring plane. The smallest makes an angle less than 2° with the C—O bond vector.

Translational tensor, **T** (Å^2)	0.0106 (3)	0.0001 (1) 0.0096 (1)	0.0008 (1) −0.0011 (1) 0.0116 (1)
Principal values (Å^2)	0.0104	0.0090	0.0123
Librational tensor, **L** (deg^2)	5.3 (2)	−1.6 (2) 6.4 (3)	−1.0 (3) 0.3 (2) 7.5 (6)
Principal values (deg^2)	4.1	6.8	8.4
Cross tensor, **S** (Å deg)	0.032 (6) −0.022 (2) −0.022 (3)	0.016 (2) 0.009 (7) −0.007 (6)	−0.022 (2) 0.002 (4) −0.023

diffraction data (Gao *et al.*, 1991). The rigid-body and mean-square displacement calculations were made using computer programs *EKRT* and *UINS* (He & Craven, 1993). The resulting modified H-atom parameters were used as fixed values in the subsequent refinement.

The charge density distribution in the crystal structure was determined by assuming the multipole pseudo-atom model of Stewart (1976). Each C, N and O pseudo-atom was represented by an invariant spherical core consisting of the Hartree–Fock K shell with two electrons and by a variable L shell represented as the terms of a complete multipole expansion up to octapoles. The spherical (monopole) L-shell term was obtained from a Hartree–Fock wavefunction with a radial function expressed as the sum of Slater functions having coefficients from Clementi & Roetti (1974). A variable radial exponent κ was introduced for each type of pseudo-atom (C, N or O) to allow for contraction or expansion of the Hartree–Fock L shell (Coppens *et al.*, 1979). Higher multipole terms were represented as single Slater functions with standard radial exponents obtained from Hehre *et al.* (1969). H atoms were represented as single Slater functions with a fixed value $\kappa = 1.24$, as recommended by Chen & Craven (1995). For H atoms, the multipole expansion involved only mono- and dipoles.

The charge density refinement was carried out by full-matrix least squares using the computer program *POP* (Craven *et al.*, 1996). The 200 variables consisted of 63 positional and U^{ij} parameters for the non-H atoms, 132 electron population parameters, three κ parameters, a scale factor applied only to the invariant pseudo-atom cores and an extinction parameter assuming the crystal to be of type (I) (Becker & Coppens, 1974). Convergence gave $R(F^2) = 0.040$, $wR(F^2) = 0.069$ and g.o.f. =

Table 3. *Interatomic distances (Å) and angles (°)*

(*a*) Intramolecular bond lengths. Columns are: (1) present study (123 K), uncorrected for librational motion; (2) present study with rigid-body librational corrections; (3) values from projection study at ambient temperature (Penfold, 1953*a*); (4) values from *ab initio* calculations (3-21G, split valence set) reported by Field & Hillier (1987).

	(1)	(2)	(3)	(4)
N1—C2	1.379 (1)	1.382	1.40	1.390
C2—O2	1.251 (1)	1.252	1.24	1.220
C2—C3	1.437 (1)	1.440	1.44	1.449
C3—C4	1.370 (1)	1.372	1.33	1.339
C4—C5	1.417 (1)	1.419	1.42	1.437
C5—C6	1.366 (1)	1.369	1.37	1.340
C6—N1	1.362 (1)	1.364	1.34	1.368

(*b*) Intramolecular bond angles

N1—C2—C3	115.0 (1)	C6—N1—H1	117.4 (1)
C2—C3—C4	121.1 (1)	C2—C3—H3	119.1 (1)
C3—C4—C5	121.0 (1)	C3—C4—H4	119.3 (1)
C4—C5—C6	117.8 (1)	C4—C5—H5	121.4 (1)
C5—C6—N1	121.0 (1)	C5—C6—H6	124.8 (1)
C2—N1—C6	124.2 (1)	N1—C2—O2	120.2 (1)
C3—C2—O2	124.8 (1)		

(*c*) Selected bond torsion angles

O2—C2—C3—C4	−177.6 (1)
O2—C2—N1—C6	177.7 (1)
N1—C2—C3—C4	2.1 (1)
C3—C2—N1—C6	−2.0 (1)

(*d*) Selected intermolecular distances and angles. Values are rounded owing to the uncertainty in the corrections for atomic thermal vibrations.

H1···O2*a*	1.78	N1···O2*a*	2.76
O2···H3*b*	2.57	O2···C3*b*	3.44
C3···H5*c*	2.83	C3···C5*c*	3.49
C4···H4*c*	2.89	C4···C4*c*	3.71
C5···H4*c*	2.79	C5···C4*c*	3.83
C6···H4*c*	2.84	C6···C4*c*	3.82
C4···H6*d*	2.88	C4···C6*d*	3.77
C5···H6*d*	2.71	C5···C6*d*	3.75
C6···H6*d*	2.70	C6···C6*d*	3.59
N1···H6*d*	2.86	N1···C6*d*	3.43
N1—H1···O2*a*	157	C6···H4*c*—C4*c*	150
O2···H3*b*—C3*b*	137	C4···H6*d*—C6*d*	139
C3···H5*c*—C5*c*	119	C5···H6*d*—C6*d*	162
C4···H4*c*—C4*c*	132	C6···H6*d*—C6*d*	139
C5···H4*c*—C4*c*	160	N1···H6*d*—C6*d*	113

Symmetry codes: (*a*) $-\frac{1}{2}-x, -y, -\frac{1}{2}+z$; (*b*) $-x, -\frac{1}{2}+y, \frac{1}{2}-z$; (*c*) $-x, -\frac{1}{2}+y, -\frac{1}{2}-z$; (*d*) $-\frac{1}{2}-x, 1-y, \frac{1}{2}+z$.

(*e*) Least-squares planes through selected atoms of the molecule. Planes are with respect to the crystal axes and are in the form $Ax + By + Cz = D$, where coefficients are in Å, and x, y and z are fractional coordinates. The planes are as follows: (1) through all atoms C, N and O of the molecule; (2) through atoms N1, C2, O2 and C3 of the peptide group; (3) through atoms C3, C4, N1 and C6 of the molecular boat-deck.

	A	*B*	*C*	*D*
(1)	9.6264	−3.0791	−2.6078	−2.0560
(2)	9.6006	−3.1625	−2.5299	−2.0640
(3)	9.6464	−3.0239	−2.6550	−2.0208

Table 3 (*cont.*)

Distances of atoms from the planes (Å)

	(1)	(2)	(3)
N1	0.018	0.000	−0.001
C2	0.005	0.001	−0.023
O2	−0.022	0.001	−0.066
C3	0.018	−0.001	0.001
C4	0.001	—	−0.001
C5	−0.021	—	−0.012
C6	0.002	—	0.001
H1	0.023	—	—
H3	0.034	—	—
H4	0.025	—	—
H5	−0.034	—	—
H6	−0.020	—	—

1.48. A final difference Fourier map showed that the residual electron density was no more than 2σ. The extinction parameter (Lorentzian mosaicity) was g = 0.29 (5) $\times 10^{-4}$ rad^{-1} assuming a spherical crystal with an average path length of 0.35 mm. The reflections 210 and 400 are most affected by extinction ($|F_o|^2/|F_{\rm kin}|^2$ = 0.91 and 0.92, respectively).† When the electron population parameters were scaled to obtain a neutral unit cell, we obtained 13.5 (1) *K*-shell and 36.5 (2) valence-shell electrons, whereas ideally a neutral molecule would have 14 *K*-shell electrons and 36 valence-shell electrons. Table 1(*a*) gives the positional and U^{ij} parameters for C, N and O atoms. The electron population and κ parameters are in Table 1(*c*). Here, all population parameters have been scaled to give a neutral molecule ($\Sigma p_v = 36$). Ellipsoidal representations of the atomic mean-square displacements (Johnson, 1976) and the atomic nomenclature are shown in Fig. 1.

3. Results and discussion

3.1. *Molecular geometry and packing*

The structure obtained at 123 K is similar to the room-temperature structure (Penfold, 1953*a*). Interatomic distances and angles are in Table 3. The molecule is planar to within ±0.02 Å (or ±0.03 Å, including the H atoms) with the ring slightly puckered into a boat form having C2 and C5 at the bow and stern (Table 3*e*). The atoms N1, C2, O2 and C3 of the *cis*-peptide group are coplanar to within 0.001 Å and this plane makes a dihedral angle of 1.9° with the plane of the boat-deck atoms N1, C6, C4 and C3, which are also coplanar to within 0.001 Å. A comparison of C—C bond lengths with those obtained from *ab initio* molecular orbital calculations (3-21G, split valence set) by Field & Hillier (1987) shows differences which are considerably greater than experimental error. The calculated values for C2—C3, C3—C4, C4—C5 and C5—C6 are 1.449, 1.339, 1.437 and 1.340 Å, whereas the corresponding experimental values (including corrections for rigid-body libration) are 1.440, 1.372, 1.419 and 1.369 Å (s.u.'s 0.001 Å). Thus, the calculated values appear to underestimate ring conjugation effects. Our results are in better agreement with the C—C bond lengths obtained for 2-thiopyridone from neutron diffraction at 123 K (Ohms *et al.*, 1982).

The molecular packing (Fig. 3) features N—H···O=C hydrogen bonding (H···O, 1.78 Å) in puckered chains parallel to the *c* direction. Planes of molecules linked by these hydrogen bonds make a dihedral angle of 124°. Thus, the cyclic dimers that have been observed in the gas phase and in solution do not occur in the crystal. In the crystal the molecules form a herringbone pattern involving all four C—H groups in molecular interactions which are near van der Waals distances or slightly shorter. The tilt of molecules related in this way is 116°. The shortest intermolecular distances (Table 3*d*) are H3···O2 (2.57 Å) and H6···C6 (2.70 Å). Corresponding heavier-atom distances are C3···O2 (3.44 Å) and C6···C6 (3.59 Å). From Fig. 3 it is seen that a C4—H4 group forms close intermolecular approaches with three C atoms at adjacent ring positions in the central molecule. On the opposite face of the central molecule a C6—H6 group makes close intermolecular approaches to the same three ring atoms and also to the N1 atom. Thus, crystals of 2-pyridone appear to involve

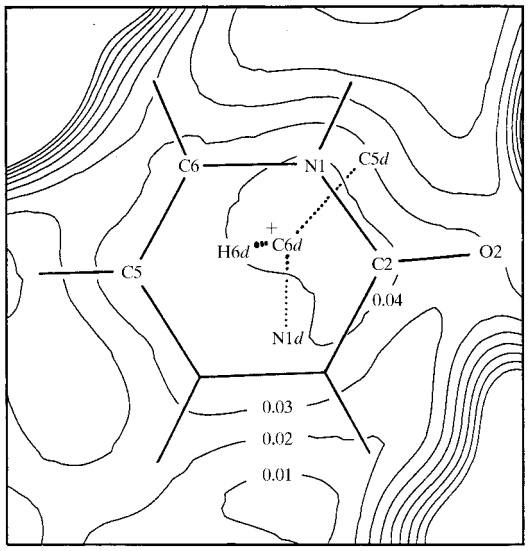

Fig. 5. The total electron density in the section parallel to the best molecular plane and passing through the C6···C6*d* critical point, which is marked by a cross. Contours are as in Fig. 4. The plane of the 2-pyridone molecule (shown with the bonds as full lines) lies 1.61 Å above the section of electron density which is shown here. Below this section dotted lines indicate part of a second molecule, including the C6—H6 group which projects towards the molecule above. The second molecule is denoted by *d* as in Tables 3 and 4 and in Fig. 3. At the critical point the electron density increases in the sections that are immediately above and below this section.

† Supplementary data for this paper are available from the IUCr electronic archives (Reference: BK0048). Services for accessing these data are described at the back of the journal.

C—H···π interactions similar to those described by Steiner *et al.* (1995).

3.2. *The charge density analysis*

The charge density distribution and other electrostatic properties for 2-pyridone have been calculated for atoms at rest making use of the parameters from Table 1 and computer programs from the *POP* system (Craven *et al.*, 1996). Thus, the total electron density in the molecular plane is shown in Figs. 4 and 5 and the corresponding Laplacian of the electron density is shown in Fig. 6. We emphasize that the prominent features in the bonding regions in Fig. 6 are absent when a Laplacian map is constructed with only the core and spherical valence-shell contributions from each atom. The electron density in Figs. 4 and 5 is contoured close to the zero level† in order to reveal the saddle-point features in the region between molecules. The most notable intermolecular bridges in Fig. 4 occur along the N—H···O hydrogen bonds between H1 and O2. They also occur along the H3···O2 region and near H4 and H6.

The total molecular electrostatic potential was obtained according to the procedure of Stewart & Craven (1994) and is shown in Fig. 7 for a molecule isolated from the crystal structure. The most prominent feature is the electronegativity of the region near the carbonyl O atom. The opposite side of the molecule is electropositive. Superposed in Fig. 7 is an arrow representing the molecular dipole moment [8.8 (19) D], which is directed 14° from the C—O bond and 2° from the molecular plane. The dipole moment reported by Albert & Phillips (1956) for 2-pyridone in dioxane solution is considerably smaller (2.95 D). Their small value could be owing to the equilibrium in solution between the monomer and the centrosymmetric dimer which has zero dipole moment (Krackov *et al.*, 1965). A larger value (4.0 D) was obtained for an isolated monomer by Field & Hillier (1987) from *ab initio* calculations. Our value is even larger, possibly because it is obtained for a molecule removed from the crystal but retaining the effects of polarization by its crystal environment.

The total electron density $\rho(\mathbf{r})$, its gradient and curvature have been analyzed according to Bader (1994), with emphasis on determining these properties at the critical points where the gradient of the density is zero [$\nabla\rho_b(\mathbf{r}) = 0$]. Critical points of special interest occur when there are saddle points between pairs of nuclear centers. At these so-called bond-critical points [designated (3, −1)], one of the principal values of the curvature is positive (λ_1), because of the increase in $\rho(\mathbf{r})$ on moving towards either nuclear center. The other two principal values (λ_2 and λ_3) are negative because $\rho(\mathbf{r})$ decreases for transverse displacements. The sum of the three curvatures gives the Laplacian, $\nabla^2\rho(\mathbf{r}) = \lambda_1 + \lambda_2 + \lambda_3$. The Laplacian at a bond-critical point may be positive or negative, depending on the relative values of λ_1 and ($\lambda_2 + \lambda_3$). A positive value for $\nabla^2\rho_b(\mathbf{r})$ corresponds

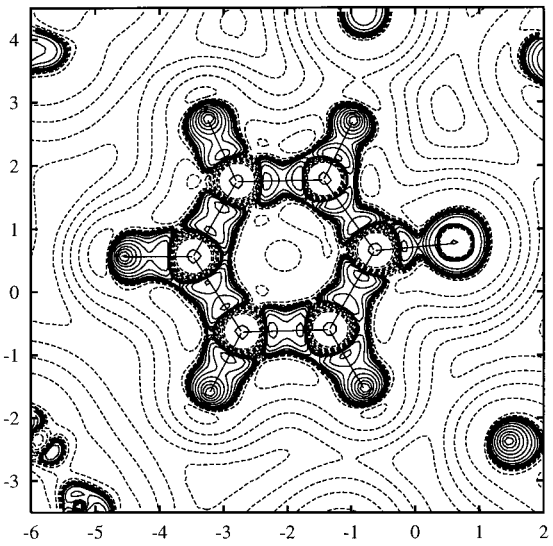

Fig. 6. The Laplacian of the total electron density for atoms at rest. The section is in the best plane of the molecule. Contours are at intervals of (0.625×2^n) e Å^{-5}, with n from 0 to 14. Solid contours are for negative regions of the Laplacian, that is, in the regions of local enhancement of the electron density. There are extreme negative and positive regions close to each atom center which are not an expression of the experimental data. The minimum resolution of the data is 0.46 Å.

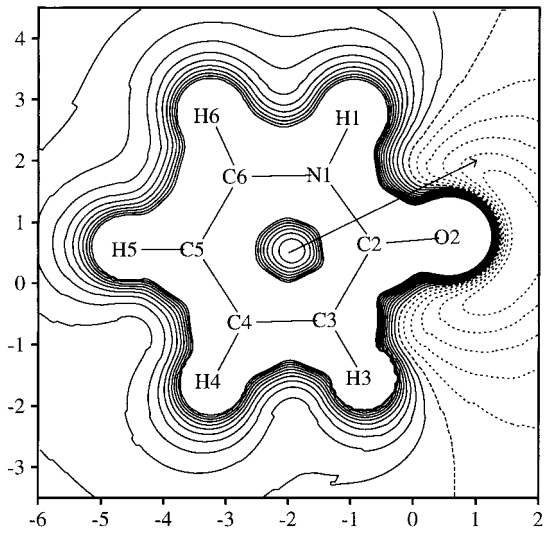

Fig. 7. The total electrostatic potential for a molecule isolated from the crystal structure. The section is in the best plane of the molecule. Contours are at 0.05 e Å^{-1}. Dashed contours represent regions of electronegativity. The arrow indicates the direction of the molecular dipole moment, $|\mu|$ = 8.8 (19) D.

† We find the most significant negative excursion of the total electron density to be −0.006 (4) e Å^{-3} at the site with fractional coordinates (−0.383, 0.191, −0.106). The electron density is positive definite throughout the sections in Figs. 4 and 5.

Table 4. *Bond-critical points*

For each bond x, y and z are the fractional coordinates ($\times 10^3$) of the critical point. The s.u.'s in the positions of the critical points range from 0.006 to 0.008 Å for intramolecular bonds and from 0.011 to 0.016 Å for the intermolecular interactions. At each critical point $\rho_b(\mathbf{r})$ (e Å^{-3}) is the charge density, $\nabla^2\rho_b(\mathbf{r})$ (e Å^{-5}) is the Laplacian, and λ_1, λ_2 and λ_3 are the three principal values of the Hessian matrix.
(*a*) Intramolecular bonds.

	x	y	z	$\rho_b(\mathbf{r})$	$\nabla^2\rho_b(\mathbf{r})$	λ_1	λ_2	λ_3
C2—C3	−104	308	50	2.01 (5)	−13.2 (11)	14.9 (5)	−12.4 (6)	−15.7 (7)
C3—C4	−66	481	−23	2.28 (6)	−20.2 (13)	13.7 (6)	−15.0 (7)	−18.8 (7)
C4—C5	−91	570	−210	1.99 (5)	−15.3 (11)	13.6 (5)	−13.1 (6)	−15.8 (7)
C5—C6	−152	474	−329	2.20 (6)	−21.9 (14)	12.1 (6)	−15.0 (6)	−19.0 (9)
C6—N1	−188	308	−266	2.36 (6)	−19.4 (14)	19.0 (7)	−17.1 (8)	−21.3 (8)
N1—C2	−161	213	−59	2.11 (6)	−16.5 (14)	15.7 (7)	−14.9 (7)	−17.3 (8)
C2—O2	−143	149	86	2.71 (8)	−35.5 (25)	15.3 (11)	−24.2 (17)	−26.7 (11)
N1—H1	−227	119	−199	2.05 (9)	−19.0 (31)	31.4 (16)	−24.7 (16)	−25.8 (17)
C3—H3	−38	400	164	1.81 (7)	−15.2 (19)	19.6 (10)	−16.9 (10)	−17.8 (10)
C4—H4	−28	657	−90	1.89 (7)	−17.7 (18)	19.1(9)	−18.0 (9)	−18.8 (11)
C5—H5	−119	649	−399	1.92 (7)	−16.8 (16)	18.3 (9)	−16.8 (8)	−18.3 (8)
C6—H6	−216	370	−444	1.88 (7)	−17.4 (19)	19.3 (10)	−17.2 (9)	−19.5 (10)

(*b*) Intermolecular interactions. The fractional coordinates are for the critical points shown in Fig. 3. Symmetry codes are as given in Table 3(*d*).

	x	y	z	$\rho_b(\mathbf{r})$	$\nabla^2\rho_b(\mathbf{r})$	λ_1	λ_2	λ_3
N1···O2*a*	−280	47	−256	0.203 (22)	4.11 (34)	6.26 (22)	−1.06 (18)	−1.09 (14)
O2···C3*b*	−51	−31	273	0.037 (5)	0.66 (7)	0.91 (5)	−0.12 (2)	−0.13 (2)
C4···C4*c*	−16	295	−234	0.036 (2)	0.47 (3)	0.55 (2)	−0.02 (1)	−0.06 (1)
C3···C5*c*	27	250	−53	0.040 (3)	0.49 (4)	0.65 (3)	−0.08 (1)	−0.08 (1)
C6···C6*d*	−236	450	−39	0.045 (3)	0.62 (4)	0.72 (2)	−0.03 (2)	−0.08 (2)

to a local depletion of electron density, with charge being displaced away from the critical point. This indicates an ionic or closed-shell interaction between the nuclear centers. Conversely, a negative value for $\nabla^2\rho_b(\mathbf{r})$ corresponds to a local accumulation of electron density indicating a covalent interaction. Other critical points include the (3, +1) type, which occurs within a ring of nuclear centers. Such a point has λ_1 and λ_2 positive and λ_3 negative.

Table 4 lists the bond-critical points. As shown in Fig. 6, all intramolecular bonds have critical points at which the Laplacian is negative, indicating that these bonds have covalent character. Furthermore, there is a small but systematic alternation in the charge density of the four C—C bonds that is consistent with differences in their bond lengths (Table 3). At the bond-critical points, the magnitudes of the electron density in the two shorter bonds C3—C4 and C5—C6 have values $\rho_b(\mathbf{r})$ = 2.28 and 2.20 (6) e Å^{-3}, which are slightly greater than $\rho_b(\mathbf{r})$ in the two longer bonds, 2.01 and 1.99 (5) e Å^{-3}. The Laplacian shows a similar effect. For the bond-critical points in the pyridone ring, differences between λ_2 and λ_3 indicate ellipticity of the charge density along the bond which is to be expected if there is π bonding around the ring. The observed differences range from 2.4 (11) e Å^{-5} for N1—C2 to 4.2 (11) e Å^{-5} for C6—N1.† The errors are too great for differences in ellipticity around the ring to be significant. The four C—H bonds have critical points with electron densities and Laplacians which are the same within experimental error.

Intermolecular interactions give rise to critical points with much smaller magnitudes for the electron density and the Laplacian. The other notable feature of all these intermolecular interactions is that the Laplacian at the critical points is positive, indicating that these are closed-shell or ionic interactions. The critical point in H1···O2 of the N—H···O hydrogen bond has the greatest electron density and Laplacian [$\rho_b(\mathbf{r})$ = 0.20 (2) e Å^{-3}, $\nabla^2\rho_b(\mathbf{r})$ = 4.1 (3) e Å^{-5}]. Magnitudes for the H3···O2 critical point in the C—H···O interaction are smaller [$\rho_b(\mathbf{r})$ = 0.037 (5) e Å^{-3}, $\nabla^2\rho_b(\mathbf{r})$ = 0.66 (7) e Å^{-5}], indicating that this interaction is considerably weaker than a conventional hydrogen bond. The values obtained for the H···O interactions in 2-pyridone are similar to those reported for 1-methyluracil (Klooster *et al.*, 1992) and for the conventional hydrogen bonds in methylammonium hydrogen succinate monohydrate (Flensburg *et al.*, 1995).

A systematic search was carried out for critical points associated with intermolecular interactions occurring on either side of the pyridone ring. The total electron density for atoms at rest was calculated in a series of sections parallel to the best least-squares ring plane (Fig. 4). The sections were contoured beginning at 0.01 e Å^{-3} and with an interval of 0.01 e Å^{-3}. Three saddle points in the electron density were found in the maps and these were refined by an iterative procedure of steepest descent in order to find each local minimum. The critical points labeled for simplicity as C4···C4*c* and C3···C5*c*

† Calculated angles between the direction of the principal curvature λ_2 at the ring bond-critical points and the normal to the plane of the pyridone ring are all less than 13° and have an average value of 7°. Thus, the orientations of ring-bond ellipticities are consistent with the effect of π bonding.

are located on the same side of the pyridone ring and C6···C6*d* is on the opposite side, as shown in the stereoview (Fig. 3). Table 4(*b*) shows that the three minima occur at about the same small but significantly non-zero electron density [0.036 (2), 0.040 (3) and 0.045 (3) e Å^{-3}]. The Laplacian at each of the three critical points shows two values which are very small (λ_2 and λ_3), indicating that the electron density is almost flat. Since the features at these three critical points are similar, we select only the C6···H6*d* interaction (Figs. 3 and 5) for more detailed discussion.

The value $\lambda_2 = -0.03$ (2) e Å^{-5} for the C6···C6*d* interaction is close to being positive. Thus, the curvatures are borderline between those of a bond-critical point and a ring-critical point. The point of minimum density is almost enclosed by a ring of higher electron density. The atoms making the greatest contribution to the electron density (and Laplacian) at the critical point are N1, C6 and C2 in the pyridone ring (0.011, 0.006 and 0.005 e Å^{-3}, respectively) and C6*d* and H6*d* of the neighboring molecule (0.010 and 0.009 e Å^{-3}). No other atoms contribute more than 0.001 Å. The arrangement of these five atoms around the critical point is shown in Fig. 5. At the critical point, although the H6*d* atom is closest (1.20 Å compared with 1.69 Å for N1, 1.89 Å for C6*d* and 1.97 Å for C2), the heavier atoms combine to make the largest contribution to the electron density. It is pointed out that while the C6*d*—H6*d* group seems to point towards the ring atom C5 and furthermore the H6*d*···C5 distance is almost as short as H6*d*···C6 (2.71 and 2.70 Å, respectively), there is no bond-critical point between H6*d* and C5. This is because the position of the critical point is more strongly influenced by C6*d* and less by H6*d* owing to the greater electron density centered at the C atom.

At first it might seem appropriate to describe the configuration around the critical point C6*d*···C6 as a C—H···π interaction (Steiner *et al.*, 1995), since it represents the interaction of the C6*d*—H6*d* group with three atoms belonging to a ring that we have shown to possess π-bonding character. However, a study of the contributions from the ring atoms C6, N1 and C2 to the electron density at the critical point shows that only the spherical components of the individual atomic valence-shell densities are involved. In our multipole model the higher multipole terms give rise to the delocalized π-bonding character around the ring, but these terms are found to be negligible at distances of ~ 1.5 Å or more above the plane of the atom centers. The ring-atom p orbitals may indeed contribute to the interaction since the product of a p_z orbital with itself gives an almost spherical electron density except near $z = 0$. Consequently, the observed charge density can be adequately described as a van der Waals interaction among spherical ring atoms.

Experimental charge density studies of very weak interactions of van der Waals type are just beginning. Efforts to locate and characterize the critical points for such interactions are thus only first steps. The finding that the electron density from more than two nuclear centers can make significant contributions at such a critical point brings fresh insights to the nature of van der Waals interactions in crystals. Crystallographers have come to describe van der Waals interactions as 'contacts', but this would appear to be inappropriate.

The study of weak interactions such as van der Waals interactions involves the region between molecules where the electron density is very small and subject to the dynamic effects of thermal vibrations, which are likely to be considerable. Thus, the static picture of weak interactions presented above gives only a snapshot of what is occurring. Nevertheless, estimates of electrostatic properties obtained here should be typical and of use for comparison with future results.

This work is supported by NIH grant No. GM-39513. We are grateful to Professor Robert F. Stewart for discussions.

References

Albert, A. & Phillips, J. P. (1956). *J. Chem. Soc.* pp. 1294–1304.
Almlöf, J., Kvick, A. & Olovsson, I. (1971). *Acta Cryst.* B**27**, 1201–1208.
Bader, R. F. W. (1994). *Atoms in Molecules: A Quantum Theory*. Oxford: Clarendon Press.
Beak, P. (1977). *Acc. Chem. Res.* **10**, 186–192.
Becker, P. J. & Coppens, P. (1974). *Acta Cryst.* A**30**, 129–147.
Blessing, R. H. (1987). *Crystallogr. Rev.* **1**, 3–58.
Chen, L. R. & Craven, B. M. (1995). *Acta Cryst.* B**51**, 1081–1097.
Clementi, E. & Roetti, C. (1974). *At. Data Nucl. Data Tables*, **14**, 177–478.
Coppens, P., Guru Row, T. N., Leung, P., Stevens, E. D., Becker, P. J. & Yang, Y. W. (1979). *Acta Cryst.* A**35**, 63–72.
Craven, B. M., Weber, H.-P., He, X., Klooster, W. T. & Yang, H. W. (1996). *The POP System: Computer Programs to Derive Electrostatic Properties from Bragg Reflections*. Technical Report, Crystallography Department, University of Pittsburgh, Pittsburgh, PA, USA.
Epstein, J., Ruble, J. R. & Craven, B. M. (1982). *Acta Cryst.* B**38**, 140–149.
Field, M. J. & Hillier, I. H. (1987). *J. Chem. Soc. Perkin Trans.* 2, pp. 617–622.
Flensburg, C., Larsen, S. & Stewart, R. F. (1995). *J. Phys. Chem.* **99**, 10130–10141.
Fujimoto, A., Inuzuka, K. & Shiba, R. (1981). *Bull. Chem. Soc. Jpn*, **54**, 2802–2806.
Gao, Q., Jeffrey, G. A., Ruble, J. R. & McMullan, R. K. (1991). *Acta Cryst.* B**47**, 742–745.
He, X. & Craven, B. M. (1993). *Acta Cryst.* A**49**, 10–22.
Hehre, W. J., Stewart, R. F. & Pople, J. A. (1969). *J. Chem. Phys.* **51**, 2657–2664.
Held, A., Champagne, B. & Pratt, D. W. (1991). *J. Chem. Phys.* **95**, 8732–8743.
Held, A. & Pratt, D. W. (1990). *J. Am. Chem. Soc.* **112**, 8629–8630.

Held, A. & Pratt, D. W. (1992). *J. Chem. Phys.* **96**, 4860–4876.
Johnson, C. K. (1976). *ORTEP*II. Report ORNL-5138. Oak Ridge National Laboratory, Tennessee, USA.
Klooster, W. T., Swaminathan, S., Nanni, R. & Craven, B. M. (1992). *Acta Cryst.* B**48**, 217–227.
Krackov, M. H., Lee, C. M. & Mautner, H. G. (1965). *J. Am. Chem. Soc.* **87**, 892–896.
Kvick, A. & Booles, S. S. (1972). *Acta Cryst.* B**28**, 3405–3409.
Kvick, A. & Olovsson, I. (1968). *Ark. Kemi*, **30**, 71–79.
Low, J. N. & Wilson, C. C. (1983). *Acta Cryst.* C**39**, 1688–1690.
Ohms, U., Guth, H., Kutoglu, A. & Scheringer, C. (1982). *Acta Cryst.* B**38**, 831–834.
Penfold, B. R. (1953*a*). *Acta Cryst.* **6**, 591–600.
Penfold, B. R. (1953*b*). *Acta Cryst.* **6**, 707–713.
Schomaker, V. & Trueblood, K. N. (1968). *Acta Cryst.* B**24**, 63–76.
Sheldrick, G. M. (1985). *SHELXS*86. *Crystallographic Computing* 3, edited by G. M. Sheldrick, C. Krüger and R. Goddard, pp. 175–189. Oxford University Press.
Steiner, T., Starikov, E. B., Amado, A. M. & Texeira-Dias, J. C. C. (1995). *J. Chem. Soc. Perkin Trans.* 2, pp. 1321–1326.
Stewart, R. F. (1976). *Acta Cryst.* A**32**, 565–574.
Stewart, R. F. & Craven, B. M. (1994). *Biophys. J.* **65**, 998–1005.